Available online at www.sciencedirect.com

SciVerse ScienceDirect

Ceramics International 39 (2013) 4263–4268

CERAMICS INTERNATIONAL

www.elsevier.com/locate/ceramint

Dielectric relaxation behaviour of Li and La co-doped NiO ceramics

A.A. Dakhel*

Department of Physics, College of Science, University of Bahrain, P.O. Box 32038, Bahrain

Received 27 May 2011; received in revised form 15 October 2012; accepted 15 October 2012
Available online 10 November 2012

Abstract

Li and La co-doped NiO ceramics have been synthesised by conventional ceramic solid-state reaction processing technique. Comprehensive structural, electrical, and dielectric studies were carried out on the samples of formula $Li_xLa_yNi_{1-x-y}O$, where $x=0.05$ and $y=0.03$ and 0.05. Their structural characterisation was carried out with X-ray diffraction. The dc electrical measurements were recorded in the temperature range 300–400 K. The dielectric properties were measured in the frequency range 0.25–100 kHz at different temperatures. At room temperature, a colossal low-frequency dielectric permittivity ($\varepsilon' \sim 10^5$–10^6) was obtained. These colossal-ε values are explained in the framework of the core/shell model. Complex-impedance spectroscopy studies on the prepared ceramics show a slight deviation from Debye-type relaxation. In general, the results of the present work suggest doping with rare earths in low concentrations to obtain colossal dielectric permittivity.

Keywords: Ceramics; Dielectric; Colossal dielectric constant; La and Li codoped NiO

1. Introduction

High permittivity NiO-based ceramics of formula $A_xB_yNi_{1-x-y}O$ (where A stands for a monvalent element such as Li, Na, K and B stands for a transition element such as Ti, Fe, V, Ta, and Al [1–5]) have been used as important components in capacitors, memory devices, and other suitable micro-electronic devices. These ceramics show colossal apparent dielectric permittivity (10^3–10^5) together with a non-perovskite and non-ferroelectric properties. Their permittivity (ε') remains almost constant around room temperature at low frequencies and rapidly decreases at sufficiently high frequencies [1,3,4,6,7]. The colossal permittivity of such materials was explained by Maxwell–Wagner (M–W) interfacial polarisation model [8,9] based on dielectric properties of micro-structural heterogeneous structure. Hence, the permittivity has two contributions: grain interiors and grain boundaries (GBs). However, the GBs are mainly responsible for the colossal dielectric permittivity [1,6,7,10]. This means that the creation of colossal ε depends on the details of the preparation conditions that control the properties of grains and grain boundary. In the present work, lanthanum as B-element was used since La oxide itself has high dielectric permittivity, good insulating properties, and low solid solubility in NiO. Indeed La^{3+} ions (of 6-coordination Shannon radius 0.1032 nm) are much larger than Ni^{2+} ions (0.069 nm [11]) and therefore, the incorporation of La^{3+} ions into NiO matrix cause a big lattice distortion. For that reason, La oxide should mainly accumulate on NiO grain boundaries and thus enhance the isolation of the grains.

In the present work, the structural and electrical properties of colossal-ε ceramics of formula $Li_xLa_yNi_{1-x-y}O$ (where $x=0.05$ and $y=0.03$ and 0.05) have been studied. The results are explained according to the core/shell model i.e. the electrically heterogeneous microstructure of the samples is the responsible for the observed colossal ε. The dopant Li^+ ions (of 6-coordination radius 0.076 nm [11]) convert NiO into a semiconductor, meanwhile the lanthanum-oxide molecules chemically bond to NiO grain surfaces. Thus, it is possible to apply the core/shell model since the interior of the grains (Li doped NiO) are semiconductor while the shells of the grains are La–rich insulating boundaries.

*Tel.: +973 1743 7455; fax: +973 1744 9148.
E-mail address: adakhil@sci.uob.bh

0272-8842/$ - see front matter © 2012 Elsevier Ltd and Techna Group S.r.l. All rights reserved.
http://dx.doi.org/10.1016/j.ceramint.2012.10.278

2. Experimental details

Pure NiO, $Li(OH)\cdot H_2O$ (Fluka A.G.), and lanthanum acetylacetonate (sigma-Aldrich) were used as starting materials. Stoichiometric amounts of starting material powders were well mixed in a small volume of methanol using an agate mortar and pestle, followed by calcination in air at 1000 °C, for about 20 h. Then, the yield powder was milled and pressed (750 MPa) into pellets 1–2 mm in thickness. Finally, these pellets were sintered in air at 1200 °C for about 20 h. The molar fraction of Li was fixed at 0.05 and two different molar fractions of La were selected to be equal or less than that of Li. Thus, the prepared ceramic discs (abbreviated as LLNO ceramic) were denoted as LLNO-1 for $Li_{0.05}La_{0.03}Ni_{0.92}O$ and LLNO-2 for $Li_{0.05}La_{0.05}Ni_{0.90}O$. The undoped NiO powder that passed the identical calcination procedure was used as reference. For electrical measurements, aluminium film electrodes were deposited on both faces of the disc-shaped samples. The samples with Al-electrodes were twice annealed at 150 °C for 2 h for good ohmic contacts. For elemental analysis of the samples, the energy dispersive X-ray fluorescence (EDXRF) spectroscopy method was used. The exciting radiation was Cu K_α and the detector was an Amptek XR-100CR detector. For the structural analysis, the X-ray diffraction (XRD) method using a Philips PW-1710 θ-2θ system with Cu K_α radiation (0.15406 nm) and scan step 0.02° was used. A thin silicon wafer was used as internal standard. The dielectric and electrical properties were measured using a Keithley 3330 LCZ instrument and Keithley model 6487 picoammeter. The ac-measurements were completed with 50 mV-signal in frequency range 250 Hz to 100 kHz.

3. Structural characterisation

Fig. 1 shows the energy dispersive XRF spectrum of the prepared LLNO ceramics. The spectrum shows Ni K_α(7.47 keV), La L_α (4.65 keV), La $L_{\beta1}$ (5.04 keV), La $L\beta_2$ (5.38 keV), and the exciting line of Cu anode. The X-ray signal from lithium was not detected with the used detector. No other significant signals were detected.

The XRD patterns of LLNO-1 and LLNO-2 are depicted in Fig. 2 together with that of the undoped NiO reference disc. All patterns show a single NiO crystalline phase that is cubic FCC (Fm3m) structure [12]. The reflection (200) has the highest intensity, as in the standard diffraction pattern. It is known that, doping of NiO with Li ions reduces the lattice parameter [13–15]. This was explained by the substitution of Ni^{2+} sites with Li^+ ions. Such doping of Li^+ ions disturbs the charge balance that must be settled by creation of oxygen vacancies, which is responsible for the reduction in lattice parameter. In contrast to Li, lanthanum (and other rare-earth elements) has small solid solubility in NiO matrix, therefore La segregates mainly on grain boundaries in form of oxide; analogous explanation was given on transition-metal

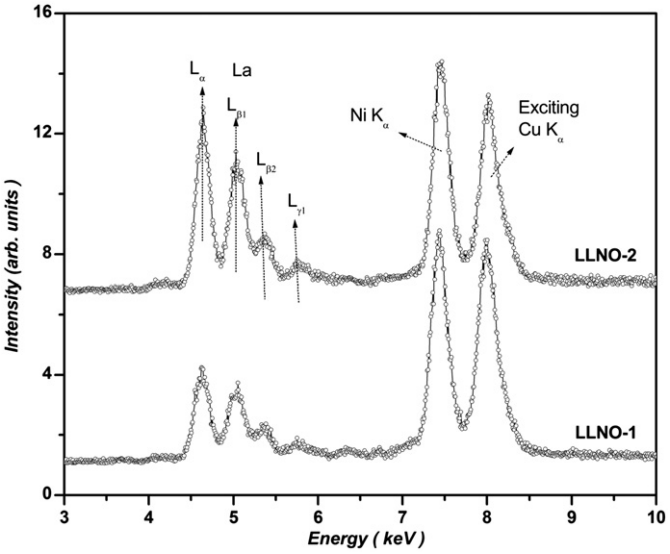

Fig. 1. XRF spectrum of LLNO-1 and LLNO-2 ceramics. The exciting radiation was Ni-filtered Cu K_α radiation.

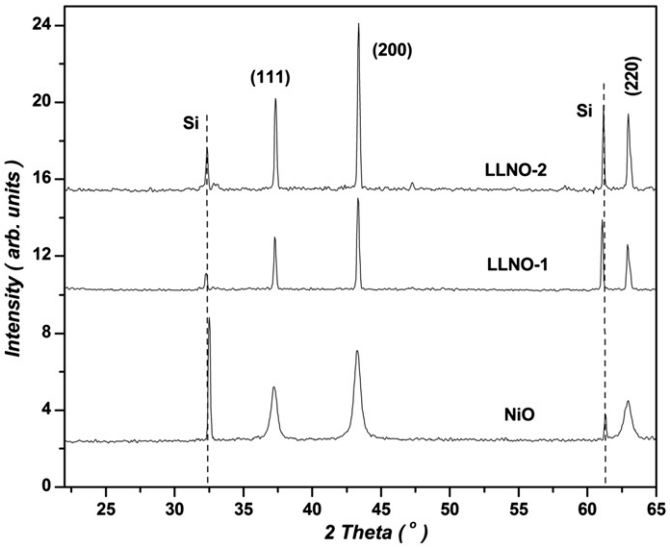

Fig. 2. XRD patterns of NiO, LLNO-1, and LLNO-2 ceramics. The radiation used was Cu K_α-line.

dopants (Ti, V, W) and Al [1,16,17], and also observed directly by scanning electron microscope (SEM) [6]. This La accumulation inhibits more doping of Li into NiO matrix i.e. inhibits more formation of NiO:Li. Therefore, the deviation (Δ) of the lattice parameter of the samples compared to undoped NiO decreases with increasing La content. The values of Δ were −0.65% and −0.57% for LLNO-1 and LLNO-2 respectively.

The "second phase" of (La–Li–O) may exist on the GBs in amorphous structure. Therefore, LLNO samples consist of Li-doped NiO grains surrounded by boundaries that contain small amounts of La and Li oxides in amorphous structure that cannot be detected by XRD technique. Consequently, the investigated samples have analogous

Table 1
X-ray Bragg angle ($2\theta_{200}$°) for (200) reflection and its half-width ([2θ°]), micro-strain (ε_s), and structural stress (σ_{st}) for the prepared reference pure undoped NiO and NiO doped with Li and La (LLNO ceramics).

Sample	$2\theta^{o}_{200}$	[2θ°]	ε_s (10^{-3})	σ_{st} (GPa)
NiO	43.587	0.28	reference	reference
LLNO-1	43.882	0.20	−6.54	2.72
LLNO-2	43.852	0.20	−5.89	2.44

microstructure to the ordinary colossal-ε materials based on NiO [1,9,17].

The half-width of the intensive (200) reflection given in Table 1 shows that the crystallinity of the sample was improved with Li doping, as observed earlier in Ref. [18]. The peak shift $\Delta(2\theta_{200})$ is caused by some structural strain ε_s ($\varepsilon_s = -\Delta\theta_{(101)}\cot\theta_{(101)}$) that was created by Li^+ doping. The micro-stress (σ_{st}) created by Li^+ doping is estimated by $\sigma_{st} \approx (3\varepsilon_s)B$, where B is the average bulk modulus of NiO (138.3 GPa [19]). Values of ε_s and σ_{st} are given in Table 1.

4. Electrical and dielectric properties

It is well known that pure and stoichiometric NiO is a Mott–Hubbard insulator of low electrical conductivity of about 10^{-13} S/cm. The non-stoichiometric NiO_{1+x} ($x \ll 1$) is known as a p-type intrinsic semiconductor. The defects that cause the hole conductivity are the "ionised Ni^{2+} ion vacancies" or [V'_{Ni}] [1,18,20]. When monvalent cations such as Li^+ is doped at the cationic site (i.e. substitution for Ni^{2+} ion [Li'_{Ni}] or °Ccupation of Ni^{2+} ion vacancy) each Li^+ is capable of donating an electron to O^{2-} and the excess of uncompensated holes boosts the p-type behaviour of NiO, thereby increasing the hole concentration [18,20]. This is energetically explained by creation of deep traps in the bandgap ($E_g \sim 4$ eV) that induces the insulating NiO to exhibit semiconducting behaviour [21].

In the present work, the conductivity of the reference NiO disc is 4.23×10^{-7} S/cm that is close to the reported range (10^{-1}–10^{-6} S/cm) usually found by many researchers [18]. This means that the calcination of the NiO disc creates structural Ni^{2+} vacancies, which slightly improves the conductivity. As observed by many researchers, the dc-electrical resistivity of NiO is strongly reduced with Li^+-doping to about ~1 Ω cm. The dc-conductivity of LLNO-1 was 1.8×10^{-3} S/cm and of LLNO-2 was 3.6×10^{-3} S/cm. Thus, the resistivity of the LLNO ceramics is much lower than that of undoped NiO. Moreover, the resistivity of LLNO ceramics decreases with increasing of temperature indicating a semiconducting behaviour as shown in the inset of Fig. 3, which gives an activation energy of 0.227 eV and 0.150 eV for LLNO-1, and LLNO-2, respectively.

The frequency dependence of dielectric permittivity of the LLNO ceramics measured in the range 250 Hz–100 kHz are shown in Fig. 4. The real part of the dielectric permittivity (ε′) shows a colossal value that is almost constant up to about

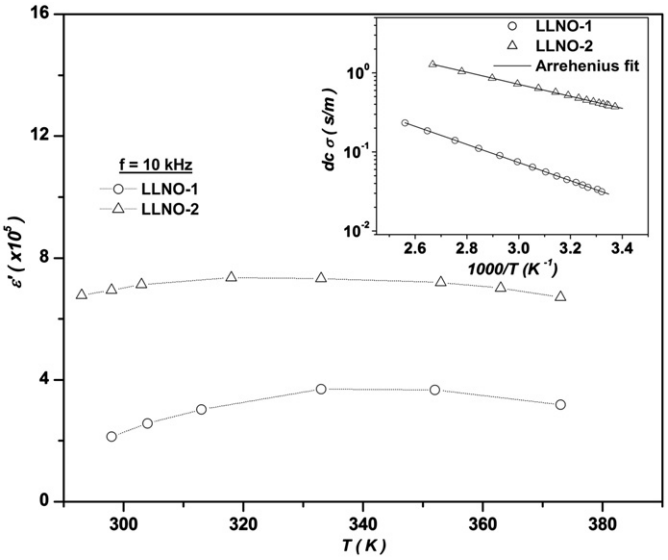

Fig. 3. Temperature dependence of dielectric permittivity, ε′ for LLNO-1 and LLNO-2 ceramics. The inset shows the Arrhenius plot of temperature dependence of dc conductivity showing the semiconducting behaviour of LLNO-1and LLNO-2 ceramics.

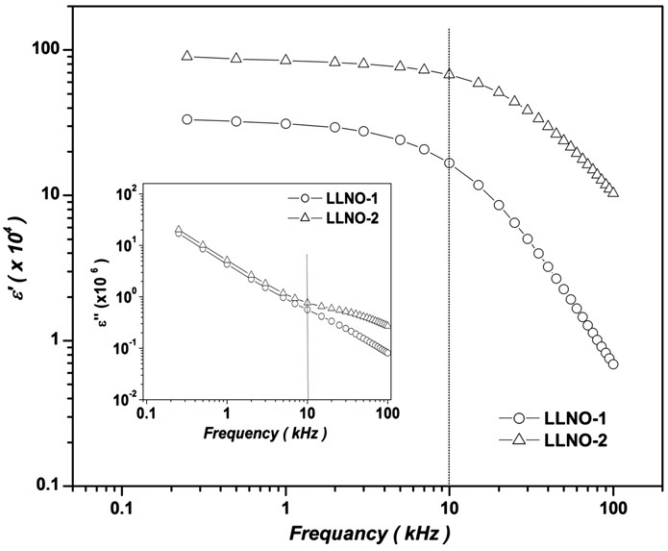

Fig. 4. Room temperature frequency dependence of dielectric permittivity, ε′ of LLNO-1 and LLNO-2 ceramics. The inset shows the frequency dependence of loss factor, ε″ of the same ceramics.

10 kHz and then rapidly decreases, especially for LLNO-1. Such behaviour with unusually large dielectric permittivity was explained by Maxwell–Wagner (MW) interfacial relaxation

mechanism, when applied to a heterogeneous system [1,3,4,9]. The MW mechanism requires existence of insulating grain boundaries (GBs). In general, the GB insulating effect is created by well-defined (distinct) GB potential barriers, which physically could be generated by a "second phase" in the sample. Such a "second phase" is formed on the GBs by the additives of La and Li oxides in the present samples. For LLNO samples, the GB construction is enhanced by more addition of La because La has low solubility in NiO.

The values of ε' at 10 kHz were 1.668×10^5 and 6.784×10^5 for LLNO-1, and LLNO-2, respectively. For comparison, the present results are larger than those values found for NiO doped with Li and Al [16]. This dielectric permittivity is about five to six orders of magnitude higher than that of undoped NiO ceramics (~30 at 1 kHz [22]). The inset of Fig. 4 shows the dependence of ε on frequency: below 10 kHz, it follows the relationship $\varepsilon'' \sim \omega^{-m}$, where m is ~0.95 for both LLNO-1 and LLNO-2 ceramics. According to the correlated barrier hopping (CBH) model, the value of m is correlated to the effective energy (W_M) of hopping over the barrier according to $m = 4k_BT/W_M$[23], where k_B is the Boltzmann constant and T is the operating temperature. The calculated value of W_M is 105 meV for both LLNO-1 and LLNO-2 ceramics. The acceptable interpretation for the application of the relation $\varepsilon'' \sim \omega^{-m}$ is that, the conduction is realised by carrier (called polaron [18]) hops between localised states [24]. In fact, this relation is consistent with Kramers–Kroning relation:$\sigma_{ac}(\omega) = \omega\varepsilon'' \sim \omega^s$.

The dielectric permittivity is weakly temperature dependent over the measured temperature range shown in Fig. 3; a similar result was also observed for other NiO-based colossal-ε materials [1,11]. The present-work colossal-ε data advises to consider doping with rare earths in low concentrations in order to obtain colossal-ε values. However, for practical applications, it is necessary to mention that the high values of the dielectric loss found in LLNO ceramics are due to relatively low resistivity.

To study the dielectric relaxation in transition element compounds, glasses, and complexes it was found that it is better to deal with dielectric modulus $M^*(\omega)$ or complex impedance $Z^*(\omega)$ rather than complex dielectric permittivity $\varepsilon^*(\omega)$ since in the latter function the actual dielectric loss (relaxation) current could be masked by the dominant conduction current [25–27]. These functions are correlated to each other according to the following relations: $M^* = j\omega C_0 Z^* = 1/\varepsilon^*$, where C_0 is the vacuum capacitance of the empty measuring cell, $\omega = 2\pi f$is the angular frequency, and$j = (-1)^{1/2}$. The complex impedance can be calculated from the following equation:

$$Z^* = Z' - jZ'' = 1/j\omega C_0\varepsilon^* = (\varepsilon'' - j\varepsilon')/[\omega C_0(\varepsilon'^2 - \varepsilon''^2)] \quad (1)$$

Fig. 5 shows the frequency dependence of Z' and Z'' for LLNO ceramics. It can be observed that $Z''(\omega)$ dependence has a maximum (peak) at ω_m where the relationship $Z'(\omega)$ becomes sensitive to the variation of frequency. The amplitude of this peak increases with increasing of La content. Such a peak indicates the incidence of relaxation

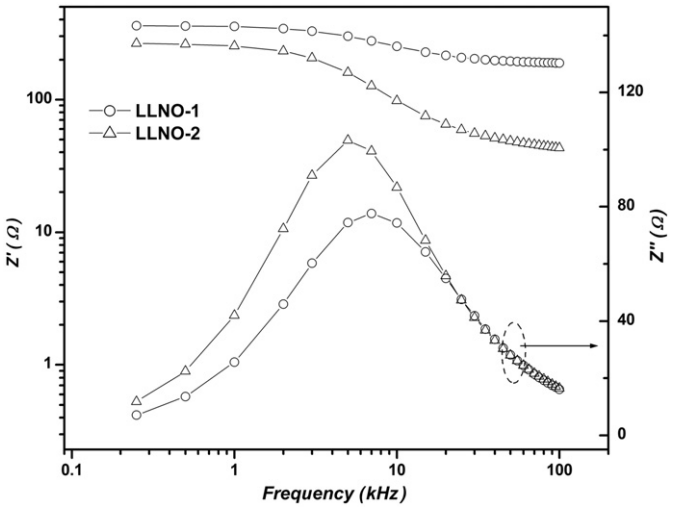

Fig. 5. Room temperature frequency dependence of real part (Z') and imaginary part (Z'') of the complex impedance for LLNO-1 and LLNO-2 ceramics.

in the ceramics of characteristic frequency ω_m. The frequency ω_m is correlated to the relaxation time τ_m through $\omega_m\tau_m = 1$[28]. The values of τ_m are 2.2×10^{-5} s and 3.1×10^{-5} s for LLNO-1 and LLNO-2, respectively. This means that the relaxation time increases with increasing La content in the sample.

The complex-impedance spectroscopy method is usually used to characterise the dielectric properties of materials and to separate out the bulk and grain boundary (GB) contributions [9]. Usually Nyquist plots (Z'vs.Z'' plot) can be analysed by using an equivalent circuit consisting of two "parallel RC elements" connecting in series. One parallel RC circuit represents the contribution of grain bulk conduction and the other represents to the distinct grain-boundary contribution. Each parallel RC circuit forms one semicircular arc in the complex Nyquist plot. The semicircle at high frequencies may be assigned to conduction within the grains and the semicircle at low frequencies may be assigned to conduction within grain boundaries (GBs). For the present experimental data, one equivalent RC circuit or one semicircle play this role. This means that the dielectric response in the present ceramics comes from one major dominant mechanism. Thus, the equivalent circuit necessary to analyse the present results is consisting of one resistance r connected in series to one parallel (RC) element, where r represents grain bulk resistance and R represents GB resistance contribution [24]:

$$Z' = r + \frac{R}{1+\omega^2C^2R^2}, Z'' = \frac{\omega CR^2}{1+\omega^2C^2R^2} \quad (2)$$

Fig. 6 shows Nyquist plots for the studied samples with semicircular fit. The frequency at which the Nyquist semicircular plot maximum occurs is determined by the time constant of the parallel RC element as described by: $\omega_m = \tau_m^{-1} = (RC)^{-1}$ [29], which is almost equal to those values of τ_m deduced from $Z''(\omega)$ curves of Fig. 5.

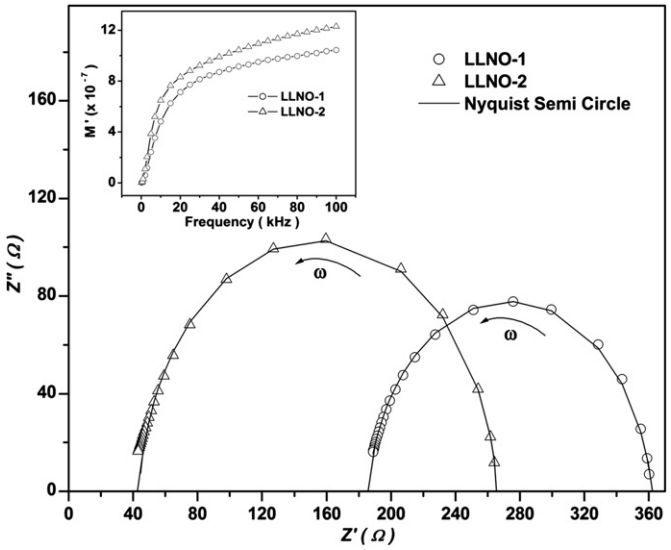

Fig. 6. Nyquist impedance plots as measured at room temperature for LLNO-1 and LLNO-2 ceramics. The lines represent the theoretical semicircles. The inset shows the room temperature frequency dependence of real part of electrical modulus M' for the same ceramics.

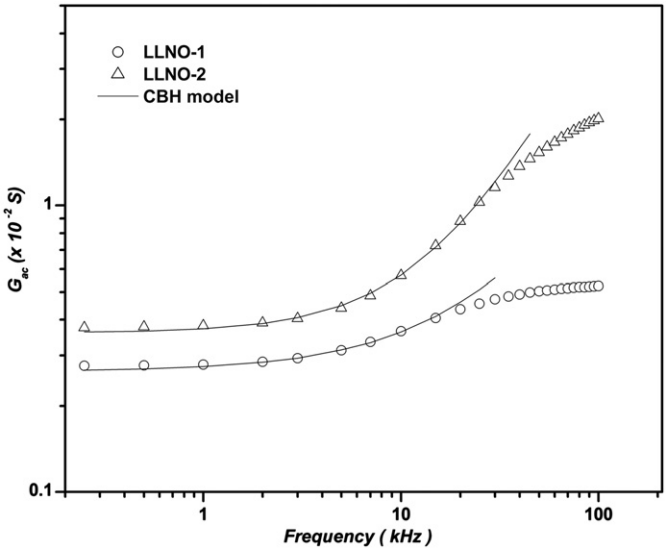

Fig. 7. Room temperature frequency dependence of ac-conductance (G_{ac}) for LLNO-1 and LLNO-2 ceramics. The lines represent the theoretical simulation according to the power-law model.

However, in Fig. 6 some points at the high-frequency side are slightly deviated from the semicircular curve pointing to the small contribution of grain bulk. On the other hand, the experimental data points are rarely found to form a full semicircle, instead forming a depressed one with its centre below the real axis. For the present data, the centres are below the Z' axis by $-8.5\,\Omega$ and $-10.8\,\Omega$ for LLNO-1, and LLNO-2, respectively. This reflects the distribution of relaxation times around the mean $\tau_m = \omega_m^{-1}$, but not a single value. Instead of using the ambiguous phenomenological constant phase element (CPE) [1], we analyse the present results according to RC model. The estimated values of R are $178.2\,\Omega$ and $229.5\,\Omega$ for LLNO-1 and LLNO-2, respectively. The sum $(r+R)$ is close to the dc-value measured directly. Thus, the addition of La increases the resistance of GBs by the accumulation of La-based compounds. It is important to mention here that, Lunkenheimer et al. [30] refer to the electrode-specimen interface polarisation effect as the origin of apparent colossal dielectric constants in such experiments. However, the disappearance of any other arc at the low frequency side of Nyquist plot indicates the possibility of neglecting the electrode-specimen interface polarisation effect [17] in the present work that is confirmed by the study of electrical modulus.

The electrical modulus M^* is a useful function to eliminate (if present) the electrode effects [24,29]. The frequency dependence of the real part of modulus (M') is shown in the inset of Fig. 6. At low frequencies, M' tends to be very small, confirming that the electrode effects make a negligible contribution and hence may be ignored when the data are analysed in modulus formalism [31,32]. At higher frequencies, M' attain a saturated (asymptotic) value $M_\infty = 1/\varepsilon_\infty$, $\varepsilon_\infty \sim 10^5 - 10^6$. In general, this demonstrates that the electrode polarisation can be neglected since it does not contribute to large dielectric values [29].

The ac conductance (G_{ac}) of insulators is often expressed according to the following relation:

$G_{ac} = G_{dc}(0) + G_{ac}(\omega)$, where $G_{dc}(0)$ is the dc-conductance of the sample and $G_{ac}(\omega)$ is the frequency-dependent component. $G_{ac}(\omega)$ is typically expressed by a power law $G_{ac}(\omega) = A_\sigma \omega^s$, where$A_\sigma$ is a coefficient [33]. According to the correlated barrier hopping (CBH) model, the exponent s is correlated to the effective barrier height for hopping $W_{M'}$that has any value smaller than the bandgap (E_g) and hence $s < 1$ [34]. $W_{M'}$ depends on the film's microstructure as the average grain size, texture orientation, defect distribution, phase content, etc. However, none of these factors were entered into the (CBH) model derived originally for uniform homogeneous non-crystalline insulators. Therefore, the experimental value of s can take any value < 1 or > 1, as it was observed in some experimental results [35,36]. The results of $s > 1$ were explained by the non-random distribution of hopping centres because of the inhomogeneity in the structural defect distribution [34] that enhances the exponent "s" by an additional factor [34,37]. Fig. 7 shows the frequency dependence of ac-conductance $G(\omega)$. The application of the above model give values s > 1 ($s \sim 1.2$). According to the CBH model, these results clearly show that the structures of the samples studied are inhomogeneous reflecting the existence of grains and GBs.

5. Conclusions

It has been found that the Li and La co-doped NiO ceramics exhibit a colossal low-frequency dielectric permittivity $\varepsilon' \sim 10^5$–10^6 that slowly varies with frequency up to about 10 kHz and almost temperature independent up to 100 °C.

Global structural and electrical investigations were conducted on samples of constant Li molar content but with different La molar content. The obtained colossal dielectric permittivity was explained by the effect of the micro-structural composition of the sample that theoretically modelled as core/shell structure. The results of the present work show that little doping of NiO with Li and La (rare earth) creates colossal dielectric permittivity.

Acknowledgement

The author wishes to thank Dr. Declan Gaynor from Royal College of Surgeons in Ireland—Medical University of Bahrain for proof reading the paper.

References

[1] J. Wu, C.W. Nan, Y. Lin, Y. Deng, Giant dielectric permittivity observed in Li and Ti doped NiO, Physical Review Letters 89 (2002) 217601.
[2] S. Maensiri, P. Thongbai, T. Yamwong, Giant dielectric response in (Li, Ti)-doped NiO ceramics synthesised by the polymerized complex method, Acta Materialia 55 (2007) 2851–2861.
[3] Y. Lin, L. Jiang, R. Zhao, C.W. Nan, High-permittivity core/shell structured NiO-based ceramics and their dielectric response mechanism, Physical Review Letters 72 (2005) 014103.
[4] P.K. Jana, S. Sarkar, B.K. Chaudhuri, Low loss giant dielectric and electrical transport behavior of $K_xTi_yNi_{1-x-y}O$ system, Applied Physics Letters 88 (2006) 182901.
[5] P.K. Jana, S. Sarkar, H. Sakata, T. Watanabe, B.K. Chaudhuri, Microstructure and dielectric properties of $Na_xTi_yNi_{1-x-y}O$ ($x=0.05$–0.30, $y=0.02$), Journal of Physics D: Applied Physics 41 (2008) 065403.
[6] B. Khumpaitool, J. Khemprasit, Improvement in dielectric properties of Al_2O_3-doped $Li_{0.30}Cr_{0.02}Ni_{0.68}O$ ceramics, Materials Letters 65 (2011) 1053–1056.
[7] Y.H. Lin, J. Wang, l. Jiang, Y. Chen, C.W. Nan, High permittivity Li and Al doped NiO ceramics, Applied Physics Letters 85 (2004) 5664.
[8] Y.J. Li, X.M. Chen, R.Z. Hou, Y.H. Tang, Maxwell–Wagner characterisation of dielectric relaxation in $Ni_{0.8}Zn_{0.2}Fe_2O_4$/$Sr_{0.5}Ba_{0.5}Nb_2O_6$ composite, Solid State Communications 137 (2006) 120–125.
[9] W.Z. Yang, M.S. Fu, X.Q. Liu, H.Y. Zhu, X.M. Chen, Giant dielectric response and mixed- valent structure in the layered-ordered double perovskite ceramics, Ceramics International 37 (2011) 2747–2753.
[10] Y.H. Lin, M. Li, C.W. Nan, J. Li, J. Wu, J. He, Grain and grain boundary effects in high-permittivity dielectric NiO-based ceramics, Applied Physics Letters 89 (2006) 032907.
[11] R.D. Shannon, Revised effective ionic radii and systematic studies of interatomic distances in halides and chalcogenides, Acta Crystallographica A32 (1976) 751–767.
[12] Powder Diffraction File, Joint Committee for Powder Diffraction Studies (JCPDS) file no.: 02-1216.
[13] Z. Li, C. Wang, X. Ma, L.Y.J. Sun, Synthesis, structures and electrochemical properties of $Li_xNi_{1-x}O$, Materials Chemistry and Physics 91 (2005) 36–39.
[14] M. Matsumiya, F. Qiu, W. Shin, N. Izu, N. Murayama, S. Kanzaki, Thin-film Li-doped NiO for thermoelectric hydrogen gas sensor, Thin Solid Films 419 (2002) 213–217.
[15] P. Kalyani, N. Kalaiselvi, Various aspects of $LiNiO_2$ chemistry: a review, Science and Technology of Advanced Materials 6 (2005) 689–703.
[16] S. Tangwancharoen, P. Thongbai, T. Yamwongb, S. Maensiria, Dielectric and electrical properties of giant dielectric (Li, Al)-doped NiO ceramics, Materials Chemistry and Physics 115 (2009) 585–589.
[17] G.J. Chen, Y.J. Hsiao, Y.S. Chang, Y.L. Chai, Structure and high dielectric permittivity of $Li_{0.01}M_{0.05}Ni_{0.94}O$ (M=V and W) ceramics, Journal of Alloys and Compounds 474 (2009) 237–240.
[18] D.P. Joseph, M. Saravanan, B. Muthuraaman, P. Renugambal, S. Sambasivam, S.P. Raja, P. Maruthamuthu, C. Venkateswaran, Spray deposition and characterisdation of nanostructures Li doped NiO thin films for application in dye-sensitized solar cells, Nanotechnology 19 (2008) 485707.
[19] Y. Makino, S. Miyake, Estimation of bulk moduli of compounds by empirical relations between bulk modulus and interatomic distance, Journal of Alloys and Compounds 313 (2000) 235–241.
[20] W.L. Jang, Y.M. Lu, W.S. Hwang, W.C. Chen, Electrical properties of Li-doped NiO films, Journal of the European Ceramic Society 30 (2009) 503–508.
[21] J. van Elp, H. Eskes, P. Kuiper, G.A. Sawatzky, Electronic structure of Li-doped NiO, Physical Review B 45 (1992) 1612–1622.
[22] Y.H. Lin, R.J. Zhao, J.F. Wang, J. Cai, C.W. Nan, Polarisation of high-permittivity dielectric NiO-based ceramics, Journal of the American Ceramic Society 88 (2005) 1808–1811.
[23] J.C. Pilet, A. Leraon, Un nouveau formalisme pour la permittivite dielectrique dans le cas d'une distribution gaussienne des temps de relaxation, Advances in Molecular Relaxation and Interaction Processes 14 (1979) 235–242.
[24] M.A.M. Seyam, Dielectric relaxation in polycrystalline thin films of In_2Te_3, Applied Surface Science 181 (2001) 128–138.
[25] M.G. Hutchins, O. Abu-Alkhair, M.M. El-Nahass, K. Abdel-Hady, Electrical conductivity and dielectric relaxation in non-crystalline films of tungsten trioxide, Journal of Non-Crystalline Solids 353 (2007) 4137–4142.
[26] R.H. Chen, R.Y. Chang, S.C. Shern, Dielectric and AC ionic conductivity investigations in $K_3H(SeO_4)_2$ single crystal, Journal of Physics and Chemistry of Solids 63 (2002) 2069–2077.
[27] A.A. Dakhel, A.Y. Ali-Mohamed, Dielectric properties of bis(2,4 pentanedionato)copper(II) crystalline films grown on Si substrate for low-k applications, Journal of Non-Crystalline Solids 355 (2009) 1264–1268.
[28] M. Ram, Electrical transport properties of $LiNiVO_4$ ceramics, Solid State Communications 149 (2009) 1226–1230.
[29] S. Manna, K. Dutta, S.K. De, High dielectric permittivity observed in Na and Al doped NiO, Journal of Physics D: Applied Physics 14 (2008) 155416.
[30] P. Lunkenheimer, V. Bobnar, A.V. Pronin, A.I. Ritus, A.A. Volkov, A. Loidl, Origin of apparent colossal dielectric constants, Physical Review B 66 (2002) 052105.
[31] F.S. Howell, R.A. Bose, P.B. Macedo, C.T. Moynihan, Electrical relaxation in a glass-forming molten salt, Journal of Physical Chemistry 78 (1974) 639–648.
[32] P.S. Anantha, K. Hariharan, AC Conductivity analysis and dielectric relaxation behaviour of $NaNO_3$–Al_2O_3 composites, Materials Science and Engineering B 121 (2005) 12–19.
[33] R.M. Hill, A.K. Jonscher, DC and AC conductivity in hopping electronic systems, Journal of Non-Crystalline Solids 32 (1979) 53–69.
[34] S.R. Elliott, AC Conduction in amorphous chalcogenide and pnictide semiconductors, Advances in Physics 36 (1987) 135–217.
[35] R.H. Chen, R.Y. Chang, S.C. Shern, Dielectric and AC ionic conductivity investigations in $K_3H(SeO_4)_2$ single crystal, Journal of Physics and Chemistry of Solids 63 (2002) 2069–2077.
[36] R.H. Chen, C.S. Shern, T. Fukami, Frequency dependence of ionic conductivity and dielectric relaxation studies in $Na_3H(SO_4)_2$ single crystal, Journal of Physics and Chemistry of Solids 63 (2002) 203–212.
[37] S.R. Elliot, E.A. Davis, Trends in defect-controlled electronic properties of group V amorphous semiconductors, Journal of Non-Crystalline Solids 35–36 (1980) 849–854.